The molecular landscape of well differentiated retroperitoneal liposarcoma

Tyler, Robert; Dilworth, Mark; James, Jonathan; Blakeway, Daniel; Stockton, Joanne; Morton, Dion; Taniere, Phillipe; Gourevitch, David; Desai, Anant; Beggs, Andrew D

DOI:
10.20944/preprints202101.0008.v1

Document Version
Early version, also known as pre-print

Citation for published version (Harvard):
Tyler, R, Dilworth, M, James, J, Blakeway, D, Stockton, J, Morton, D, Taniere, P, Gourevitch, D, Desai, A & Beggs, AD 2021, *The molecular landscape of well differentiated retroperitoneal liposarcoma*. MDPI. https://doi.org/10.20944/preprints202101.0008.v1

 doi:10.20944/preprints202101.0008.v1

The molecular landscape of well differentiated retroperitoneal liposarcoma

Robert Tyler[1], Mark P Dilworth[1], Jonathan James[1], Daniel Blakeway[1], Joanne D Stockton[1], Dion G. Morton[1], Phillipe Taniere[2], David Gourevitch[2], Anant Desai[2], Andrew D Beggs[1]

1 = Institute of Cancer and Genomic Medicine, College of Medical and Dental Sciences, University of Birmingham

2 = Midland Abdominal Retroperitoneal Sarcoma Unit (MARSU), University Hospital Birmingham

Address for correspondence:

Andrew Beggs

Institute of Cancer & Genomic Science

University of Birmingham

Vincent Drive

Birmingham

B15 2TT

Email: a.beggs@bham.ac.uk

Keywords: Liposarcoma, whole genome sequencing, RNA sequencing, methylation

Additional information:

Funding: The work was partially funded by a pump priming grant from the Cancer Research UK Birmingham Experimental Cancer Medicine Centre. AB acknowledges funding from the Wellcome Trust (102732/Z/13/Z), Cancer Research UK (C31641/A23923) and the Medical Research Council (MR/M016587/1).

Data statement: Sequencing and microarray data is available for access in the European Genome Phenome Archive (ref: XXX)

Acknowledgments: We thank Illumina UK (Miao He, Sean Humphray, Mahesh Vasipalli, Zoya Kingsbury and David Bentley) for sequencing and bioinformatics support for this project.

 doi:10.20944/preprints202101.0008.v1

Competing financial interests: The authors declare they have no competing financial interests

Author contribution statement:

Sample collection and patient recruitment: ADB, AD, DG

Histopathological analysis and IHC: PT, ADB

Sample processing & DNA/RNA extraction: ADB, MPD, JJ, DB, JDS

Validation sequencing: ADB, MPD, JJ, DB, JDS

Data analysis: ADB

Manuscript: ADB, MPD, JJ, DB, JDS, DGM, PT, DG, AD.

Preprints (www.preprints.org) | NOT PEER-REVIEWED | Posted: 4 January 2021 doi:10.20944/preprints202101.0008.v1

ABSTRACT

Well differentiated liposarcoma (WD-LPS) is a relatively rare tumour, with less than 50 cases occurring per year in the UK. These tumours are both chemotherapy and radiotherapy resistant and present a significant treatment challenge requiring radical surgery. Little is known of the molecular landscape of these tumours and no current targets for molecular therapy exist. We aimed to carry out a comprehensive molecular characterisation of WD-LPS via whole genome sequencing, RNA-sequencing and methylation array analysis. A recurrent mutation within exon1 of *FOXD4L3* was observed (chr9:70,918,189A>T; c.322A>T; p. Lys108Ter). Recurrent mutations were also observed in Wnt signalling, immunity, DNA repair and hypoxia-associated genes. Recurrent amplification of *HGMA2* was observed, although this was in fact part of a general amplification of the region around this gene. Recurrent gene fusions in *HGMA2*, *SDHA*, *TSPAN31* and *MDM2* were also observed as well as consistent rearrangements between chromosome 6 and chromosome 12. Our study has demonstrated a recurrent mutation within *FOXD4L3*, which shows evidence of interaction with the PAX pathway to promote tumorigenesis.

Preprints (www.preprints.org) | NOT PEER-REVIEWED | Posted: 4 January 2021 doi:10.20944/preprints202101.0008.v1

INTRODUCTION

Retroperitoneal liposarcoma (RPLS) is the most common type of retroperitoneal sarcoma (RPS), making up around a half of all RPS (1). RPLS typically presents incidentally on cross-sectional imaging as a large homogenous retroperitoneal mass (2). As these tumours become larger, the risk of their transformation from well-differentiated to de-differentiated increases. The molecular events that initiate WD-LPS and lead to de-differentiation of well differentiated liposarcoma are currently unknown. Molecular changes seen in the various types of RPLS include co-ordinated amplification of MDM2 and CDK4 (3), giant ring chromosomes (4-6), amplification of *CDK4*, *HMGA2* and *TSPAN31* and the *FUS-DDIT3* fusion oncogene, seen in a subset of liposarcomas caused by t(12:16) or (t12:22) translocation (7, 8). To date, there have been few comprehensive studies on the molecular genetics of well differentiated RPLS (9). The key feature is amplification of the *MDM2* gene which has been seen almost ubiquitously in WD-RPLS and DD-RPLS at rates approaching 100% (10). In an exome sequencing study, Kanojia et al (11) found consistent amplification as previously described in MDM2 and HGMA2. The most frequently mutated gene in their cohort was in PLEC (27% of samples), which codes for plectin, a cytoskeleton protein. Amin-Mansour et al (12) studied exome sequencing trios of normal, well differentiated and dedifferentiated tissue regions in patients with liposarcoma, finding no common driver but verifying the recurrent amplification of *CDK4*.

However, the lack of a comprehensive integrated analysis means that therapeutic options for treatment of this tumour are limited as the molecular pathways that are potentially dysregulated in liposarcoma have not been identified with certainty. We therefore

Preprints (www.preprints.org) | NOT PEER-REVIEWED | Posted: 4 January 2021 doi:10.20944/preprints202101.0008.v1

carried out a comprehensive a pilot multi-platform molecular characterisation, utilising whole genome sequencing, RNA sequencing and methylation arrays of well differentiated retroperitoneal liposarcoma

Preprints (www.preprints.org) | NOT PEER-REVIEWED | Posted: 4 January 2021 doi:10.20944/preprints202101.0008.v1

METHODS

Sample collection

Retroperitoneal sarcoma samples were obtained from patients undergoing laparotomy for en-bloc excision of retroperitoneal mass. Immediately after the specimen was removed from the patient, it was conveyed to the Queen Elizabeth Hospital Birmingham Histopathology laboratories where a representative sample of liposarcoma and associated normal fat was taken, and immediately flash frozen in liquid nitrogen and then stored at -80C. Where no normal fat was available, normal adjacent organ (i.e. kidney/colon/pancreas etc.) were sampled. Where no frozen material was available to match with the specimen, formalin fixed, paraffin embedded tissue blocks were retrieved from the histopathology archives of the Queen Elizabeth Hospital, Birmingham.

Ethical approval was obtained via the University of Birmingham Human Biomaterials Resource Centre Biobanking ethics (Ref 09/H1010/75). All experiments were performed in accordance with relevant guidelines and regulations and informed consent was obtained from all participants.

DNA/RNA extraction

Preprints (www.preprints.org) | NOT PEER-REVIEWED | Posted: 4 January 2021 doi:10.20944/preprints202101.0008.v1

DNA extraction was performed by Proteinase K digestion. A 5mm^3 piece of tissue was immersed in buffer ATL overnight with 20mg proteinase K. The resulting lysate was processing using the Qiagen DNEasy Blood & Tissue kit (Qiagen UK). Extracted DNA was eluted into buffer AL and was quantified using Nanodrop spectrophotometry for purity and Qubit (Thermo Scientific, UK) fluorimetry for DNA concentration.

Because of limited volumes of tissue, RNA extraction was performed on formalin fixed, paraffin embedded sections. Three 10μM FFPE sections were cut using a microtome then processed using the Purelink FFPE RNA extraction kit (Invitrogen) as per manufacturer's instructions. Extracted RNA was quantified for purity using Nanodrop spectrophotometry and for quantity using Qubit fluorimetry.

Whole genome sequencing (WGS) & targeted sequencing

Shotgun WGS was performed using 500ng of paired tumour:normal DNA by the Illumina R&D group at the Illumina Great Chesterford facility. DNA was library prepared for sequencing using the Truseq PCR free library preparation kit as per manufacturers guidelines. For six samples (associated normal), no fresh frozen material was available and therefore a PCR based whole genome sequencing library preparation was used (Illumina FFPE) using 1μg of DNA. Sequencing performed on an Illumina

Preprints (www.preprints.org) | NOT PEER-REVIEWED | Posted: 4 January 2021 doi:10.20944/preprints202101.0008.v1

HiSeq 2500 pooling one sample across four lanes using the v4 chemistry. Sequenced reads were aligned to the GrCh37 reference genome using the Isaac aligner (13). Tumour-normal SNV and indel calling was performed using the Strelka variant caller(14). Copy number variant calling was performed in Canvas in tumour-normal mode, and in where no control normal was available, a panel of normals were used. Structural variant calling was performed using Manta.

In order to resolve complex variants and paralogues, targeted nanopore sequencing of the *FOXD4L3* region was carried out. Custom primers were designed with Primer3 to target the entire coding sequence of FOXD4L3 in one amplicon. A long range PCR (conditions available on request) was performed and PCR amplicons cleaned and ligated using an Oxford Nanopore ligation sequencing kit (LSK-109). Library was then loaded onto a ONT MinIon 9.5.1 flow cell and run for 36 hours. Data was base called using Guppy and variant calling performed by MiniMap2. No polishing was performed.

Whole genome sequencing data for the well differentiated liposarcoma line 93T449 was downloaded from the NCBI SRA archive. Downloaded data was aligned to the GRCh38 reference genome using MiniMap2, then variant calling was performed with FreeBayes and copy number calling with Canvas as previously described.

RNA sequencing

Preprints (www.preprints.org) | NOT PEER-REVIEWED | Posted: 4 January 2021 doi:10.20944/preprints202101.0008.v1

Whole transcriptome sequencing using 1μg of total RNA was performed by the Shenzen Research Laboratories of Beijing Genomics Inc using the Illumina TruSeq RNA Sample preparation kit v2. RNA was DNAase digested, fragmented and cDNA was synthesised using SuperScript III (Invitrogen). cDNA was then end-repaired, A-tailed, adapter ligated, PCR amplified and purified. After library quantification, this was treated with duplex specific nuclease (Evrogen) and purified. The final libraries were sequenced on an Illumina HiSeq 2000 to an average of 35 million reads with a read length of 90bp.

Sequenced reads were quality trimmed using Trimmomatic, and aligned with the hg38 reference genome using STAR(15). Absolute gene expression was determined using *featureCounts* (16) and differential expression was determined using the GSA module of Partek Flow (17, 18).Log normalised FPKM values were submitted to the CIBERSORT immune infiltrate pipeline (19) for deconvolution of immune cell types and were used to calculate the Coordinate Immune Response Cluster (CIRC) score(20)
RNA fusion analysis was carried out using the fusion analysis pipeline of STAR-FUSION(21).

DNA methylation arrays

Analysis of the methylome was achieved using Illumina Human Methylation450 arrays at the University of Birmingham. One microgram of DNA was bisulphite converted using the Zymo EZ-DNA methylation kit using the custom Illumina microarray protocol.

Preprints (www.preprints.org) | NOT PEER-REVIEWED | Posted: 4 January 2021 doi:10.20944/preprints202101.0008.v1

This was then hybridised to Illumina HumanMethylation450 microarrays according to the manufacturers' protocol. Hybridised arrays were washed and stained, and then immediately scanned using an Illumina iScan microarray scanner. Extracted microarray intensities were normalised using the *Bioconductor/ChAMP* pipeline (22) and individual beta values exported. Differential methylation was quantified using *eBayes/limma* and differentially methylated regions ascertained using *DMRhunter.*

Further bioinformatics analysis

Identification of recurrent somatic mutations was carried out as follows. Firstly, exported subtracted tumour-normal variant calls from Strelka were transformed from Variant Call Files (VCF) to MAF (Mutation Annotation File) using vcf2maf. In patients were no matched normal was available, tumour VCF files were filtered using dbSNP 1000 Genomes project and GnoMAD such that all SNPs with a minor allele frequency of greater than 0.01 were discarded. MAF files were then concatenated together in order for analysis in MutSigCV (23). Analysis of recurrent mutations in the cohort was carried out using MutSigCV using standard settings. All recurrent mutations were ranked and sorted by p-value.

Identification of recurrent structural variations was carried out using the Manta (24) structural variant caller (https://github.com/Illumina/manta). The package was run with standard parameters on tumour BAM files. Subsequent output was

Preprints (www.preprints.org) | NOT PEER-REVIEWED | Posted: 4 January 2021 doi:10.20944/preprints202101.0008.v1

then filtered to produce Circos (RCircos) plots by taking a subset of the data from Manta and limiting it to intrachromosomal inversions and translocations.

Copy number alterations were called using the Illumina Canvas (25) (https://github.com/Illumina/canvas) copy number variant caller. The package was run with standard parameters on tumour BAM files. Regions were output as standard VCF files and then filtered using a custom script to preserve high quality copy number calls (quality score >30) on regions greater than 5 kilobases in length (as this was thought to be more functionally relevant). Copy number calls were then imported into GREVE (26) (http://www.well.ox.ac.uk/GREVE/) with genome-wide plots and chromosome level significance plots output.

Preprints (www.preprints.org) | NOT PEER-REVIEWED | Posted: 4 January 2021 doi:10.20944/preprints202101.0008.v1

Validation of findings

Sanger sequencing to validate mutational findings was carried out using standard methodology. Primers flanking the region of interest were designed using Exon Primer with a T_m of 60ºC. Primer specificity was verified using UCSC in-silico PCR and primers were optimised with gradient PCR before use. 10ng of tumour DNA underwent PCR using the Qiagen Multiplex kit using primers against *FOXD4L3* (supplementary table 6). PCR products were cleaned with ExoSAP-IT and underwent a BigDye sequencing reaction under standard conditions. Sequencing products were run on an ABI 3700 sequencer.

Nanopore sequencing was carried out via long range PCR of the entire FOXD4L3 gene in one amplicon. A master mix was prepared containing template DNA, 2 µL of forwards and reverse primers at 0.4 µM, 25 µL LongAmp Taq 2X Master Mix (New England Biolabs, USA) and nuclease-free water up to a total of 50 µL. Thirty cycles of long range PCR (with a 2.5 minute extension time at 65ºC) were performed and the product underwent repair and end prep using the Oxford Nanopore LSK-109 sequencing protocol. Samples were indexed with the Rapid Barcoding Kit and then loaded and sequenced on an R9.4.1 MinIon flow cell for 24 hours. Raw sequence FAST5 files were demultiplexed and converted to FASTQ using the Guppy Base caller. Called FASTQ files underwent two rounds of polishing with Canu followed by a round of polishing with Medaka. Sequence data was aligned using

Preprints (www.preprints.org) | NOT PEER-REVIEWED | Posted: 4 January 2021 doi:10.20944/preprints202101.0008.v1

minimap2 to the GRCh38 genome followed by variant calling using FreeBayes (command line *freebayes -C 2 -0 -O -q 20 -z 0.10 -E 0 -X -u -p 2 -F 0.6*). Raw allele counts at the desired sites were output with the samtools command.

RESULTS

A total of eight WD-LPS samples underwent whole genome sequencing of three tumour:normal pairs and five tumour only samples (due to lack of available paired normal tissue, to an average of 85x read depth), RNA transcriptomic sequencing of tumours only (average 35 million reads per sample) and analysis on the HumanMethylation450 array system. The characteristics of the patients from which tumour samples were obtained are shown in Table 1.

Whole genome sequencing reveals recurrent mutations in FOXD4L3

Mutational rate in all tumours was between 1.65-1.8 mutations/mega base, making WDLPS a relatively infrequently mutated tumour to others studied in the TCGA. Analysis of recurrent mutations using MutSigCV2 within the samples demonstrated significant mutations (Table 2, Figure 1) in *SPRN*, *FOXD4L3*, *ADH1C* and *KRTAP2-2*. Pathway analysis of these gene mutations determined that only *FOXD4L3* was likely to be relevant in a cancer context due to it being a Forkhead transcription factor associated gene. *FOXD4L3* was predicted by the STRINGS database (supplementary table 1) to interact with *PAX3*, *PAX7*, *T* and *TBX19*, transcription factors all involved in cell differentiation and development, as well as being implicated in alveolar rhabdomyosarcoma (27). We also analysed recurrently mutated genes within the Cancer Gene Census and those previously reported in liposarcoma

Preprints (www.preprints.org) | NOT PEER-REVIEWED | Posted: 4 January 2021 doi:10.20944/preprints202101.0008.v1

(11) using the Illumina Encore pipeline (Supplementary figure 1) including immune evasion (*HLA-A*, 5/8 samples), Wnt signalling (FAT1;4/8 samples), double strand break repair (ATM, 2/8 samples; BRCA1 2/8 samples), PAX transcription factor (PAX5, 2/8 samples) and hypoxia tumour suppressors (SDHA, 2/8 samples).

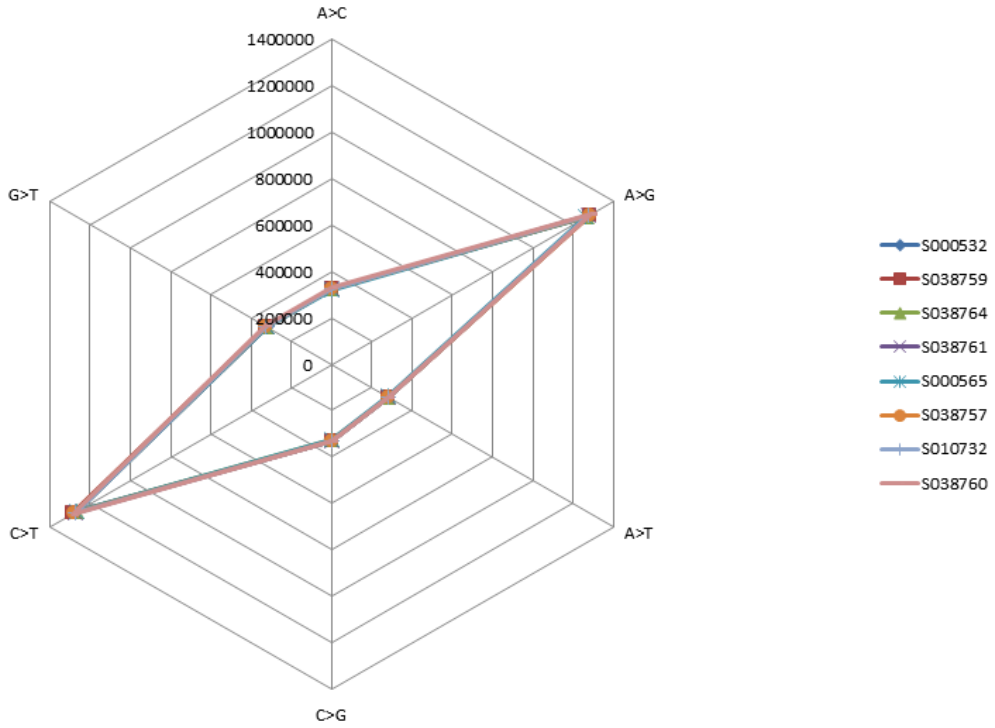

We therefore studied *FOXD4L3* in more details and found a recurrent mutation with exon 1 of *FOXD4L3* (chr9:70,918,189A>T; c.322A>T; p.Lys108Ter) which resulted in a stop gain. This mutation was present in 7/8 samples and was verified by bidirectional

Preprints (www.preprints.org) | NOT PEER-REVIEWED | Posted: 4 January 2021 doi:10.20944/preprints202101.0008.v1

Sanger sequencing of tumour samples, however this mutation was also present in two normal samples (patients P001224 and P001207) but not in a further normal sample (P001193). The mutation seen in the normal tissue as determined by NGS was not seen on Sanger sequencing. Further investigation revealed that the “normal” tissue was in fact “normal” fat immediately adjacent to the tumour. The mutation was just upstream of the Forkhead box domain of the protein (Supplementary Figure 2), suggesting that this mutation may have functional consequences due to loss of this protein binding domain.

Because of the incongruity between the whole genome sequencing and the Sanger sequencing results, we decided to carry out further investigation. *FOXD4L3* is a paralogue of *FOXD4* and has multiple (six) paralogues, with minimal sequence variation between them. We therefore designed long range PCR primers to flank the entirety of *FOXD4L3* and performed long range nanopore amplicon sequencing on a cohort of 24 FFPE samples (consisting of 12 tumour samples plus 12 adjacent normal tissues) plus the 3TL3 liposarcoma cell line. We found that the variant allele frequency of the A>T transversion was significantly different between tumour and normal tissue with the tumour having a median VAF of the T allele of 0.43 (IQR 0.39-0.45) and the normal tissue having a median VAF of 0.21 (IQR 0.16-0.22, Wilcoxon rank $p < 0.001$). Investigation of the 93T449 well differentiated liposarcoma cell line revealed a copy number (CN) = 3 of the regions surrounding the FOXD4L3 gene which was replicated in the whole genome sequenced samples, suggesting a complex mutation and copy number event within FOXD4L3 giving the differences in allele frequency.

Preprints (www.preprints.org) | NOT PEER-REVIEWED | Posted: 4 January 2021 doi:10.20944/preprints202101.0008.v1

Copy number analysis of WGS confirms recurrent gains in MDM2 as part of a larger amplification

Copy number variant analysis of the tumour set (Table 6), demonstrated the recurrent copy number gain in *HGMA2*, the binding partner of *MDM2* (28), in six out of eight cases. Recurrent amplification was seen (Figure 3) throughout the long arm of Chr12q13.13-q24.33 demonstrating that it is not necessarily restricted to the MDM2/HGMA2 amplification previously described. Analysis of structural variation (SV) revealed a complex pattern (Supplementary Figure 5) of small scale chromosomal translocation across the tumour types. Re-arrangement of both between and within chromosomes 6 and 12, was seen (Supplementary figure 6), consistent which previous cytogenetic observation of WD-LPS .

RNA sequencing demonstrates changes in fat associated genes and downregulation of Wnt and PI3K signalling

Differential expression analysis between liposarcoma and normal fat was carried out in Partek flow (Supplementary table 6). The most differentially expressed gene was *TNS1* (Tensin 1, normalised counts 20.54 vs. 110.9, p=2x10-6, Q=0.03), which is part of the PTEN signalling pathway. Pathway analysis however demonstrated dysregulated pathways in “Pathways in Cancer” (hsa05200, ES

Preprints (www.preprints.org) | NOT PEER-REVIEWED | Posted: 4 January 2021 doi:10.20944/preprints202101.0008.v1

11.61, p=9.1x10-6), MAPK signalling pathway (hsa04010, ES 6.49, p=1.52x10-3) and PI3K-Akt signalling (hs04151, ES 5.26, p=5.21x10-3).

Analysis of alternative splicing was carried out using STAR (Supplementary table 7), with *FN1* (fibronectin 1) being the top ranked alternatively spliced gene (Normalised counts tumour = 10.28, normal=0.41; p=4.52x10-9, Q=8.25x10-6. Pathway analysis demonstrated the focal adhesion pathway was significantly alternatively spliced (hsa04510, ES=18.22, p=1.22x10-8).

CIBERSORT analysis of genes associated with immune cell infiltration was carried out and showed that liposarcoma has variable immune cell infiltration, with all samples having some degree of T-cell infiltration, suggesting some degree of recognition of the tumour by the immune system (Supplementary table 8).

Gene fusion analysis demonstrates a recurrent fusion in SDHA which causes loss of activity.

Gene fusion prediction (Table 3) via analysis of WGS data demonstrated recurrent fusion events in *HGMA2*, *SDHA*, *TSPAN31*, *MDM2* and *WIF1*. *HGMA2* (28) , *TSPAN31* and *MDM2* (9) amplification/fusion have been well described in liposarcoma, however SDHA (succinate dehydrogenase complex flavoprotein subunit A) has not previously been identified, with 11 fusions in 4 samples in this dataset. In order to validate this, we then carried out RNA fusion analysis using a targeted RNA panel analysis on a

Preprints (www.preprints.org) | NOT PEER-REVIEWED | Posted: 4 January 2021 doi:10.20944/preprints202101.0008.v1

separate set of 24 FFPE samples (12 tumour/12 associated normal) as previously described. This validated (Supplementary table 9) a recurrent fusion in *SDHA* in 8/12 samples, between exon 12 of *SDHA* and exon 8 of *SLC9A3*.

Methylation analysis shows dysregulation of metastasis suppression

We then carried out methylome analysis using the Illumina HumanMethylation 450 array. The top differentially methylated gene (Supplementary table 4) was *ANKAR* (cg06479433, $\%meth_{tumour}$ = 95.0, $\%meth_{normal}$=74.1%, p_{adj}=2.59x10-10, BF = 19.01. Analysis of differentially methylated regions demonstrated six differentially methylated regions that met a genome wide significance level of $1x10^{-6}$ (table 4). The most significant DMR was *TIMP2* (tissue metalloproteinase 2) which acts as a metastasis suppressor by suppression of the Wnt/β-catenin pathway (29). We observed an average increase in methylation across the region of 35% which would suggest *TIMP2* becomes inactivated, thus dysregulating Wnt. Two DMRs were in CpG islands approximately 5kb upstream of *FOXC1* (a Forkhead box gene of unknown function, implicated in both breast (30) and small cell lung cancer (31)) and *HOXD3* (a homeobox gene responsible for growth and differentiation (32))

Gene set enrichment analysis of the DMPs was carried out, which demonstrated significant enrichment of gene sets associated with cancer, with the top ranked gene set being “FARMER_BREAST_CANCER_CLUSTER_5”, AUC=0.84, p=2.94x10-7.

 doi:10.20944/preprints202101.0008.v1

Preprints (www.preprints.org) | NOT PEER-REVIEWED | Posted: 4 January 2021 doi:10.20944/preprints202101.0008.v1

CONCLUSIONS

We have demonstrated a recurrent loss of function mutation in the *FOXD4L3* gene, a Forkhead box gene. This is in contrast to other studies (11), which suffered from poor coverage of *FOXD4L3*, a mixed sample set. A significant weakness of our study is the lack of paired normal tissues for all samples, which may cause low frequency or rare mutant alleles to not be detected due to germline variation, however we were limited by available tumour material because of the site and size of the tumour.

The *FOXD4L3* gene is within a complex region of an ancestral duplication site (33) in chromosome 9 that is postulated to have occurred early in hominid evolution. Although the sequence similarity is high (34) between the different paralogs of FOXD4 (approximately > 95%) the principle difference between paralogs is the presence of an indel leading to frameshift, either a 1-bp deletion at codon 292 or a 53-bp deletion at codon 363 causing alternate protein products to be produced. We observed a stop gain mutation at codon 260, well upstream of the previously described deletions, within the Forkhead binding domain, supported by Sanger sequencing primers specific for *FOXD4L3*. This mutation has been observed in dbSNP 147 (rs7021123) from ExAC data, however at extremely low frequency (MAF = 0.00825) in one subject only. We did not observe any RNA sequencing reads that aligned to *FOXD4L3*, despite it being expressed in normal fat on the Illumina Human BodyMap 2.0 database. Typically, a premature stop codon would cause nonsense mediated decay (NMD) of the product after the initial round of translation, however as *FOXD4L3* is a single exon gene we cannot with certainty point to NMD as the mechanism here

Preprints (www.preprints.org) | NOT PEER-REVIEWED | Posted: 4 January 2021 doi:10.20944/preprints202101.0008.v1

We successfully demonstrated the previously identified (11) recurrent copy number change in HGMA2, the binding partner of MDM2, as part of amplification of a larger region on the long arm of chromosome 12 rather than an effect specific to HGMA2 .

Our matched RNAseq analysis showed dysregulation in both the PI3K-AKT and MAPK pathways, as well as genes associated with the transition away from fat to a “tumour” phenotype. Methylation analysis of these tumours demonstrated activation of pro-apoptotic genes and genes associated with metastasis. The recurrent fusion within *SDHA* is also of interest, as similar genes (SDHB in paraganglioma (35) and SDHC in gastrointestinal stromal tumours (36)) are implicated in tumorigenesis.

Further study and functional models are required to understand the effect of changes in these genes and their relevance in WD-LPS as well as the consequences and effects of *FOXD4L3* mutation in association with WDLPS, however multiple potential target pathways for therapy have now been identified.

REFERENCES

1. Crago AM, Singer S. Clinical and molecular approaches to well differentiated and dedifferentiated liposarcoma. Current opinion in oncology. 2011;23(4):373-8.

2. Pasquali S, Vohra R, Tsimopoulou I, Vijayan D, Gourevitch D, Desai A. Outcomes Following Extended Surgery for Retroperitoneal Sarcomas: Results From a UK Referral Centre. Annals of surgical oncology. 2015.

3. Dei Tos AP, Doglioni C, Piccinin S, Sciot R, Furlanetto A, Boiocchi M, et al. Coordinated expression and amplification of the MDM2, CDK4, and HMGI-C genes in atypical lipomatous tumours. The Journal of pathology. 2000;190(5):531-6.

4. Micci F, Teixeira MR, Bjerkehagen B, Heim S. Characterization of supernumerary rings and giant marker chromosomes in well-differentiated lipomatous tumors by a combination of G-banding, CGH, M-FISH, and chromosome- and locus-specific FISH. Cytogenetic and genome research. 2002;97(1-2):13-9.

5. Pedeutour F, Suijkerbuijk RF, Van Gaal J, Van de Klundert W, Coindre JM, Van Haelst A, et al. Chromosome 12 origin in rings and giant markers in well-differentiated liposarcoma. Cancer genetics and cytogenetics. 1993;66(2):133-4.

6. Pedeutour F, Forus A, Coindre JM, Berner JM, Nicolo G, Michiels JF, et al. Structure of the supernumerary ring and giant rod chromosomes in adipose tissue tumors. Genes, chromosomes & cancer. 1999;24(1):30-41.

7. Riggi N, Cironi L, Provero P, Suva ML, Stehle JC, Baumer K, et al. Expression of the FUS-CHOP fusion protein in primary mesenchymal progenitor cells gives rise to a model of myxoid liposarcoma. Cancer research. 2006;66(14):7016-23.

 doi:10.20944/preprints202101.0008.v1

8. Kabjorn Gustafsson C, Stahlberg A, Engtrom K, Danielsson A, Turesson I, Aman P. Cell senescence in myxoid/round cell liposarcoma. Sarcoma. 2014;2014:208786.

9. Conyers R, Young S, Thomas DM. Liposarcoma: molecular genetics and therapeutics. Sarcoma. 2011;2011:483154.

10. Thway K, Flora R, Shah C, Olmos D, Fisher C. Diagnostic utility of p16, CDK4, and MDM2 as an immunohistochemical panel in distinguishing well-differentiated and dedifferentiated liposarcomas from other adipocytic tumors. The American journal of surgical pathology. 2012;36(3):462-9.

11. Kanojia D, Nagata Y, Garg M, Lee DH, Sato A, Yoshida K, et al. Genomic landscape of liposarcoma. Oncotarget. 2015;6(40):42429-44.

12. Amin-Mansour A, George S, Sioletic S, Carter SL, Rosenberg M, Taylor-Weiner A, et al. Genomic Evolutionary Patterns of Leiomyosarcoma and Liposarcoma. Clin Cancer Res. 2019;25(16):5135-42.

13. Raczy C, Petrovski R, Saunders CT, Chorny I, Kruglyak S, Margulies EH, et al. Isaac: ultra-fast whole-genome secondary analysis on Illumina sequencing platforms. Bioinformatics. 2013;29(16):2041-3.

14. Saunders CT, Wong WS, Swamy S, Becq J, Murray LJ, Cheetham RK. Strelka: accurate somatic small-variant calling from sequenced tumor-normal sample pairs. Bioinformatics. 2012;28(14):1811-7.

15. Liao Y, Smyth GK, Shi W. The Subread aligner: fast, accurate and scalable read mapping by seed-and-vote. Nucleic acids research. 2013;41(10):e108.

16. Liao Y, Smyth GK, Shi W. featureCounts: an efficient general purpose program for assigning sequence reads to genomic features. Bioinformatics. 2014;30(7):923-30.

17. Law CW, Chen Y, Shi W, Smyth GK. voom: Precision weights unlock linear model analysis tools for RNA-seq read counts. Genome biology. 2014;15(2):R29.

18. Ritchie ME, Phipson B, Wu D, Hu Y, Law CW, Shi W, et al. limma powers differential expression analyses for RNA-sequencing and microarray studies. Nucleic acids research. 2015;43(7):e47.

19. Chen B, Khodadoust MS, Liu CL, Newman AM, Alizadeh AA. Profiling Tumor Infiltrating Immune Cells with CIBERSORT. Methods Mol Biol. 2018;1711:243-59.

20. Lal N, Beggs AD, Willcox BE, Middleton GW. An immunogenomic stratification of colorectal cancer: Implications for development of targeted immunotherapy. Oncoimmunology. 2015;4(3):e976052.

21. Haas BJ, Dobin A, Li B, Stransky N, Pochet N, Regev A. Accuracy assessment of fusion transcript detection via read-mapping and de novo fusion transcript assembly-based methods. Genome biology. 2019;20(1):213.

22. Morris TJ, Butcher LM, Feber A, Teschendorff AE, Chakravarthy AR, Wojdacz TK, et al. ChAMP: 450k Chip Analysis Methylation Pipeline. Bioinformatics. 2014;30(3):428-30.

23. Lawrence MS, Stojanov P, Polak P, Kryukov GV, Cibulskis K, Sivachenko A, et al. Mutational heterogeneity in cancer and the search for new cancer-associated genes. Nature. 2013;499(7457):214-8.

24. Chen X, Schulz-Trieglaff O, Shaw R, Barnes B, Schlesinger F, Kallberg M, et al. Manta: rapid detection of structural variants and indels for germline and cancer sequencing applications. Bioinformatics. 2016;32(8):1220-2.

25. Roller E, Ivakhno S, Lee S, Royce T, Tanner S. Canvas: versatile and scalable detection of copy number variants. Bioinformatics. 2016.

26. Cazier JB, Holmes CC, Broxholme J. GREVE: Genomic Recurrent Event ViEwer to assist the identification of patterns across individual cancer samples. Bioinformatics. 2012;28(22):2981-2.

27. Begum S, Emami N, Cheung A, Wilkins O, Der S, Hamel PA. Cell-type-specific regulation of distinct sets of gene targets by Pax3 and Pax3/FKHR. Oncogene. 2005;24(11):1860-72.

28. Italiano A, Bianchini L, Keslair F, Bonnafous S, Cardot-Leccia N, Coindre JM, et al. HMGA2 is the partner of MDM2 in well-differentiated and dedifferentiated liposarcomas whereas CDK4 belongs to a distinct inconsistent amplicon. International journal of cancer Journal international du cancer. 2008;122(10):2233-41.

29. Xia Y, Wu S. Tissue inhibitor of metalloproteinase 2 inhibits activation of the beta-catenin signaling in melanoma cells. Cell cycle. 2015;14(11):1666-74.

30. Jensen TW, Ray T, Wang J, Li X, Naritoku WY, Han B, et al. Diagnosis of Basal-Like Breast Cancer Using a FOXC1-Based Assay. Journal of the National Cancer Institute. 2015;107(8).

31. Wei LX, Zhou RS, Xu HF, Wang JY, Yuan MH. High expression of FOXC1 is associated with poor clinical outcome in non-small cell lung cancer patients. Tumour biology : the journal of the International Society for Oncodevelopmental Biology and Medicine. 2013;34(2):941-6.

32. Chen LN, Rubin RS, Othepa E, Cer C, Yun E, Agarwal RP, et al. Correlation of HOXD3 promoter hypermethylation with clinical and pathologic features in screening prostate biopsies. The Prostate. 2014;74(7):714-21.

33. Fan Y, Newman T, Linardopoulou E, Trask BJ. Gene content and function of the ancestral chromosome fusion site in human chromosome 2q13-2q14.1 and paralogous regions. Genome research. 2002;12(11):1663-72.

34. Fan Y, Linardopoulou E, Friedman C, Williams E, Trask BJ. Genomic structure and evolution of the ancestral chromosome fusion site in 2q13-2q14.1 and paralogous regions on other human chromosomes. Genome research. 2002;12(11):1651-62.

35. Neumann HP, Pawlu C, Peczkowska M, Bausch B, McWhinney SR, Muresan M, et al. Distinct clinical features of paraganglioma syndromes associated with SDHB and SDHD gene mutations. Jama. 2004;292(8):943-51.

36. Pantaleo MA, Astolfi A, Urbini M, Nannini M, Paterini P, Indio V, et al. Analysis of all subunits, SDHA, SDHB, SDHC, SDHD, of the succinate dehydrogenase complex in KIT/PDGFRA wild-type GIST. Eur J Hum Genet. 2014;22(1):32-9.

Preprints (www.preprints.org) | NOT PEER-REVIEWED | Posted: 4 January 2021 doi:10.20944/preprints202101.0008.v1

FIGURE LEGENDS:

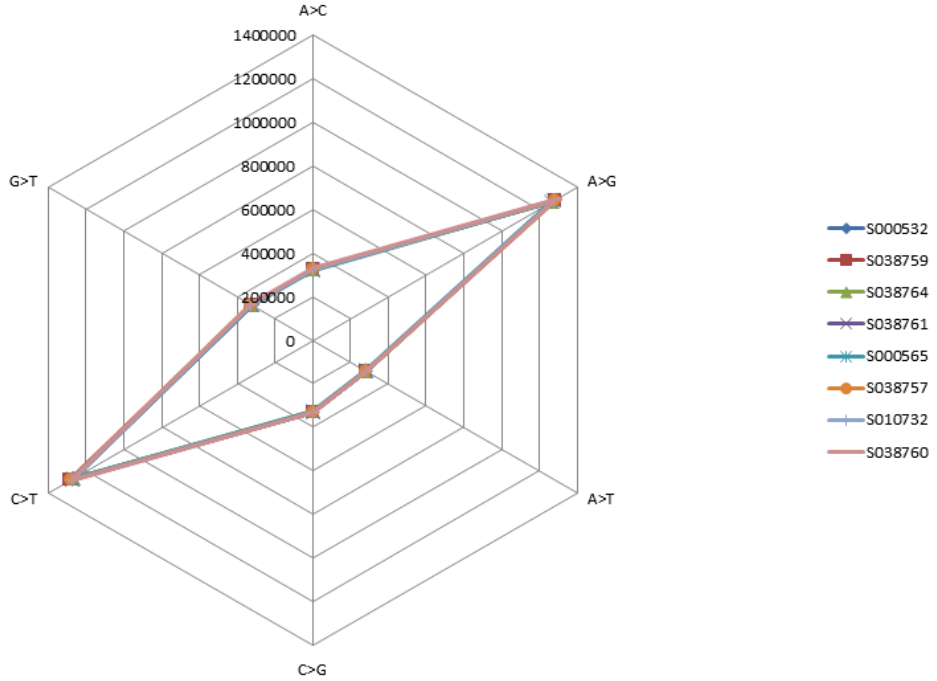

Figure 1: Spider chart of mutation type in whole genome sequencing data

Preprints (www.preprints.org) | NOT PEER-REVIEWED | Posted: 4 January 2021 doi:10.20944/preprints202101.0008.v1

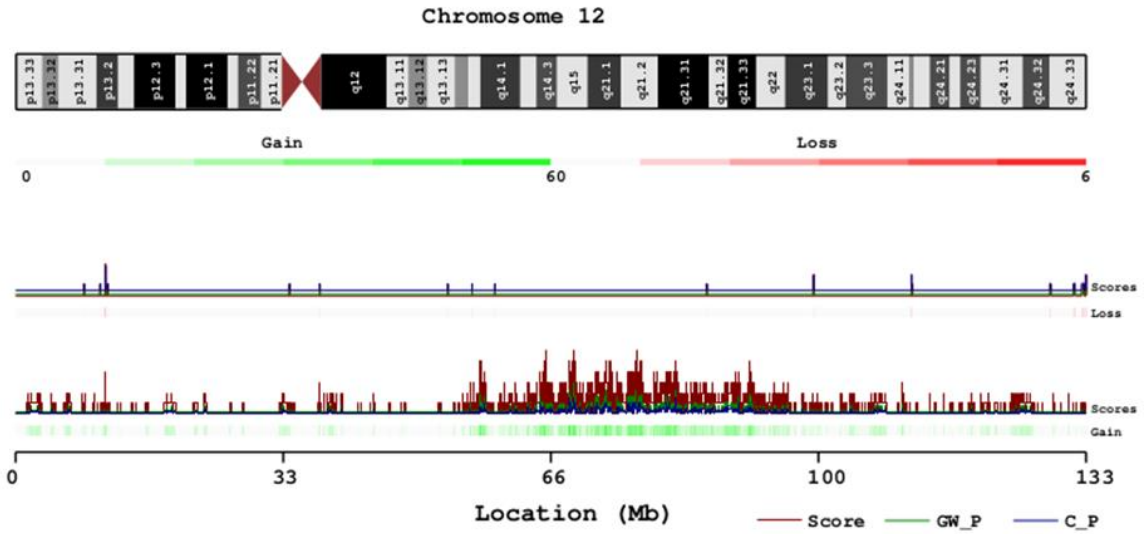

Figure 2: Chromosomal ideogram showing chromosomal gains/losses in chromosome 12

Preprints (www.preprints.org) | NOT PEER-REVIEWED | Posted: 4 January 2021 doi:10.20944/preprints202101.0008.v1

TABLES:

Table 1: Table of patient characteristics

Patient ID	Sample ID	Type	Gender	Age	Tumour location	Tumour histological type	Patient alive?
P000111	S000532	TUMOUR	Male	59	Retroperitoneum	Well differentiated liposarcoma	Alive
P000214	S000565	TUMOUR	Male	76	Retroperitoneum	Well differentiated liposarcoma	Deceased
P001190	S038759	TUMOUR	Female	63	Retroperitoneum	Well differentiated liposarcoma	Alive
P001193	S038757	TUMOUR	Female	81	Retroperitoneum	Well differentiated liposarcoma	Deceased
	S038758	NORMAL	Female	81	Retroperitoneum	Normal fat	Deceased
P001207	S010732	TUMOUR	Female	60	Retroperitoneum	Well differentiated liposarcoma	Deceased
	S044139	NORMAL	Female	60	Retroperitoneum	Normal fat	Deceased
P001212	S038764	TUMOUR	Male	58	Retroperitoneum	Well differentiated liposarcoma	Alive
P001224	S010732	TUMOUR	Female	63	Retroperitoneum	Well differentiated liposarcoma	Deceased
	S038770	NORMAL	Female	63	Retroperitoneum	Normal fat	Deceased

Preprints (www.preprints.org) | NOT PEER-REVIEWED | Posted: 4 January 2021 doi:10.20944/preprints202101.0008.v1

P001216	S038761	TUMOUR	Male	79	Retroperitoneum	Well differentiated liposarcoma	Deceased

Table 2: List of mutations ranked by significance

Rank	Gene	Gene name	p-value	q-value	Significant
1	SPRN	Shadow Of Prion Protein Homolog	8.21E-09	1.55E-04	Yes
2	ADH1C	Alcohol dehydrogenase 1C	1.52E-07	1.43E-03	Yes
3	FOXD4L3	Forkhead box D3 Like 3	2.57E-07	1.62E-03	Yes
4	KRTAP2-2	Keratin Associated Protein 2-2	2.04E-06	9.63E-03	Yes
5	LILRB3	Leukocyte Immunoglobulin-Like Receptor, Subfamily B	3.37E-06	1.27E-02	No
6	GYPE	Glycophorin-E	8.26E-05	2.60E-01	No
7	GOLGA8B	Golgin A8 Family, Member B	1.22E-04	3.28E-01	No
8	OR2A42	olfactory receptor family 2 subfamily A member 42	2.05E-04	4.82E-01	No
9	IL7R	Interleukin 7 Receptor	2.52E-04	4.82E-01	No
10	C12orf77	Chromosome 12 Open Reading Frame 77	2.68E-04	4.82E-01	No

Table 3: List of gene fusions as predicted by WGS

Gene	**Chromosome**	**Gene start**	**Gene end**	**no. fusion**	**no. sample**	**Sample ID**
HMGA2	12	66217911	66360075	4	4	S000565, S038759, S038764, S038761
HLA-A	6	29909037	29913661	7	4	S000532, S000565, S038764, S038761
SDHA	5	218356	256815	11	4	S010732, S000565, S038759, S038764

Preprints (www.preprints.org) | NOT PEER-REVIEWED | Posted: 4 January 2021 doi:10.20944/preprints202101.0008.v1

TSPAN31	12	58131796	58143994	3	2	S010732, S038761
ESR1	6	151977826	152450754	4	2	S038758, S010732
CDC73	1	193091147	193223031	2	1	S038761
ERC1	12	1099675	1605099	2	1	S038761
NCOR2	12	124808961	125052135	2	1	S000565
SUFU	10	104263744	104393292	2	1	S038761
MYH11	16	15797029	15950890	3	1	S000565
NOTCH1	9	139388896	139440314	3	1	S038761
TPR	1	186280784	186344825	3	1	S038761
MDM2	12	69201956	69239214	5	1	S000565
WIF1	12	65444406	65515346	5	1	S000565
AFF3	2	100162323	100759201	17	1	S038761

Table 4: List of significantly differentially methylated regions in WDLPS

Rank	Gene ID	Gene feature	Chr	Start of DMR	End of DMR	Size of DMR in bp	Change in percent methylation	P-value for DMR	Name of gene	Function

Preprints (www.preprints.org) | NOT PEER-REVIEWED | Posted: 4 January 2021 doi:10.20944/preprints202101.0008.v1

1	TIMP2	3'UTR_shore	17	76850012	76850463	452	-35%	1.71E-08	Tissue Inhibitor of Metalloprotineases 2	Metastasis suppressor
2	C22orf9	Body_none	22	45607945	45609196	1252	39%	2.42E-08	Chromosome 22 open reading frame 9	Lysine acetylation
3	SLC44A4	TSS200_none	6	31846943	31847023	81	-25%	1.13E-07	Solute carrier family 44 member 4	Overexpressed in prostate cancer
4	NA	IGR_shore	6	1601197	1601541	345	-34%	1.29E-07	CpG island 5kb upstream of FOXC1	
5	NA	IGR_shelf	2	177020321	177024020	3700	-29%	6.73E-07	CpG 4kb upstream of near HOXD3	
6	BCL2L15	Body_none	1	114429332	114430298	967	-40%	7.11E-07	BCL2-Like 15	Proapoptotic gene

Table 5: Recurrent copy number events

Chr	Type	Start	End	Size in b.p.	Position (hg19 coordinates)	Samples present in	Score	Genome-wide p-value	Chromosome-wise P-value	Gene
chr1	Loss	152555501	152586848	31347	chr1:152555501-152586848	6	0.75	7.44E-15	2.22E-16	*LCE3C, LCE3B*
chr1	Loss	210078101	210085706	7605	chr1:210078101-210085706	6	0.75	7.44E-15	2.22E-16	*NA*
chr2	Loss	98153590	98162215	8625	chr2:98153590-98162215	6	0.75	7.44E-15	2.22E-16	*ANKRD36B*
chr2	Loss	146862601	146876770	14169	chr2:146862601-146876770	6	0.75	7.44E-15	2.22E-16	*NA*

Preprints (www.preprints.org) | NOT PEER-REVIEWED | Posted: 4 January 2021 doi:10.20944/preprints202101.0008.v1

chr3	Loss	68739701	68747751	8050	chr3:68739701-68747751	6	0.75	7.44E-15	2.22E-16	*NA*
chr8	Loss	8073170	8086655	13485	chr8:8073170-8086655	6	0.75	7.44E-15	2.22E-16	*NA*
chr12	Gain	66225201	66235890	10689	chr12:66225201-66235890	6	0.75	1.78E-13	3.25E-09	*HGMA2*
chr15	Gain	20832601	20844600	11999	chr15:20832601-20844600	6	0.75	1.78E-13	2.12E-14	*NA*
chr15	Gain	22344037	22344161	124	chr15:22344037-22344161	6	0.75	1.78E-13	2.12E-14	*Antibody heavy chains*
chrX	Loss	115138001	115152874	14873	chrX:115138001-115152874	6	0.75	7.44E-15	5.03E-11	*NA*